CHARACTERIZING THE SMALL SCALE STRUCTURE IN CLUSTERS OF GALAXIES

NASA Grant NAG5-3065

Final Report

For the Period 1 October 1995 through 30 September 2000

Principal Investigator
Dr. William R. Forman

March 2001

Prepared for:

National Aeronautics and Space Administration
Goddard Space Flight Center
Greenbelt, Maryland 20771

Smithsonian Institution
Astrophysical Observatory
Cambridge, Massachusetts 02138

The Smithsonian Astrophysical Observatory
is a member of the
Harvard-Smithsonian Center for Astrophysics

The NASA Technical Officer for this grant is Dr. Donald West, Code 684.1, Laboratory for Astronomy and Solar Physics, Space Sciences Directorate, NASA/Goddard Space Flight Center, Greenbelt, MD 20771

We studied galaxy clusters Abell 119, Abell 754, and Abell 1750, using data from the ASCA and ROSAT satellites (see Novicki, Jones, & Donnelly in American Astronomical Society Meeting 193, 38.07). These three clusters were chosen from a larger sample based on large temperature gradients in their temperature profiles and non-uniform distributions in their X-ray intensities. Abell 119 has a cool region in the northeast, with temperatures decreasing toward the southwest. Abell 754 shows evidence for a shock in its temperature maps. Abell 1750 also shows evidence for a shock, located between two of the three components of the cluster. All of these exhibited signs of merger activity within their central region, as well as evidence for possible large scale ($\sim$ 1 Mpc) filamentary structure. These filaments may represent the preferred direction of accretion into these clusters.

In addition, we completed the paper "Merging Binary Clusters" (see attached). This paper analyzed three clusters which appeared to be rather tightly bound and in the process of merging. These three clusters, A3528, A1750 and A3395, each exhibited bimodal structure. Since the sub-clusters in these systems have projected separations of 0.93, 1.00 and 0.67 Mpc respectively, we combined X-ray and optical observations to investigate their dynamics. Using data taken with *ROSAT* and *ASCA*, we analyzed the temperature and surface brightness distributions. We also included velocity distributions of the three clusters using new measurements supplemented with previously published data. We examined both the overall cluster properties as well as the individual sub-concentrations in each cluster. These results were then applied to the determination of the overall cluster masses, that showed excellent consistency between the various methods used. While the characteristic parameters of the sub-clusters are typical of isolated objects, our temperature results for the regions between the two sub-clusters clearly confirm the presence of merger activity that is suggested by the surface brightness distributions.

TO BE SUBMITTED TO *The Astrophysical Journal*
Preprint typeset using LaTeX style emulateapj v. 04/03/99

MERGING BINARY CLUSTERS

R. HANK DONNELLY[1], W. FORMAN[1], C. JONES[1], H. QUINTANA[2], A. RAMIREZ[3], E. CHURAZOV[4,5], M. GILFANOV[4,5]

to be submitted to The Astrophysical Journal

ABSTRACT

We study three prominent bi-modal X-ray clusters: A3528, A1750 and A3395. Since the sub-clusters in these systems have projected separations of 0.93, 1.00 and 0.67 Mpc respectively, we examine their X-ray and optical observations to investigate the dynamics and possible merging of these sub-clusters. Using data taken with *ROSAT* and *ASCA*, we analyze the temperature and surface brightness distributions. We also analyze the velocity distributions of the three clusters using new measurements supplemented with previously published data. We examined both the overall cluster properties as well as the two sub-cluster elements in each. These results were then applied to the determination of the overall cluster masses, that demonstrate excellent consistency between the various methods used. While the characteristic parameters of the sub-clusters are typical of isolated objects, our temperature results for the regions between the two sub-clusters clearly confirm the presence of merger activity that is suggested by the surface brightness distributions. These three clusters represent a progression of equal-sized sub-cluster mergers, starting from initial contact to immediately before first core passage.

Subject headings: galaxies: clusters: individual (A1750, A3395, A3528, SC0627-54) — galaxies:ICM — X-rays: galaxies

1. INTRODUCTION

Optical and X-ray studies (e.g. Forman et al. 1981; Geller & Beers 1982; Jones & Forman 1984; Dressler & Shectman 1988; Mohr et al. 1995; Bird 1994; Slezak et al. 1994) have shown that galaxy clusters are dynamically evolving systems, exhibiting a variety of substructure and asymmetric morphologies. The high frequency of substructure – $\sim$ 40% (Forman & Jones 1990)– suggests that clusters are still forming hierarchically through the merger and accretion of subclusters and galaxy groups. While the prevalence of substructure has primarily been used to constrain cosmologies (Richstone, Loeb, & Turner 1992; Mohr et al. 1995), detailed studies of merging clusters impact a number of important areas including cooling flow formation and evolution, galaxy evolution, and gravitational mass measurements.

Temperature maps of the X-ray emitting gas are an especially sensitive tool for the detection of dynamic activity. Hydrodynamic simulations indicate that mergers should produce characteristic temperature patterns that survive 4-6 times longer than perturbations in the gas density (e.g. Schindler & Müller 1993; Ricker 1997). Recent observations (e.g. Henry & Briel 1995; Henriksen & Markevitch 1996; Markevitch et al. 1996a, 1998; Donnelly et al. 1998, Markevitch et al. 2000) have found just such characteristic temperature structures in a variety of clusters. In particular, in the earliest stages of a merger, simulations show the development of a shock located be-

[1]Harvard-Smithsonian Center for Astrophysics, 60 Garden Street, Cambridge, MA 02138, USA
[2]Department of Astronomy and Astrophysics, Pontificia Universidad Catolica de Chile, Casilla 104, Santiago 22, CHILE
[3]Department of Physics, Universidad de La Serena, Benavente 980, La Serena, CHILE
[4]Space Research Institute (IKI), Moscow 117810, RUSSIA
[5]Max Planck Institute für Astrophysik, 85740 Garching bei München, GERMANY

tween the two subclusters and significant heating of the local ICM (Evrard 1990a and b; Schindler & Müller 1993).

Abell 3528, Abell 1750 and Abell 3395 are known as canonical binary galaxy clusters (Forman et al. 1981, Raychaudury et al. 1991). All three exhibit two clearly separated peaks of emission in X-rays, and varying degrees of distortion in their X-ray surface brightness suggesting a progressive sequence of merging.

We used X-ray data from the *ROSAT* and *ASCA* satellites to characterize the emission profile of the gas as well as to map the distribution of temperatures and fit specific regions of interest with typical spectral models. We also analyzed optical velocity measurements to study the internal kinematics and overall dynamics of each cluster.

In Section 2 we discuss the data, its reduction and present the basic results of our work. Section 3 gives estimates of the masses determined from fitting the emission intensity profile, the X-ray luminosity and a virial estimate based on the velocities of the galaxies. Finally, we discuss the implications of our results in Sections 4 and 5 respectively. Throughout the paper we assumed $H_0 = 65$ km s^{-1} Mpc^{-1}, and the error bars quoted on all results are at the 1 σ level.

2. OBSERVATIONS & METHODS

All three clusters– A3528, A1750, and A3395– were observed using both *ROSAT* and *ASCA*. The data were obtained from the HEASARC public archives and the details of the observations are given in Table 1. Using the broad energy response of *ASCA* (0.5-10.0 keV), these observations were used to accurately measure the gas temperatures and distributions in these clusters. The significantly better spatial resolution of *ROSAT* was used to determine the cluster surface brightness distribution and the *ROSAT* spectra of the central regions provided a diagnostic for the presence of cooling flows.

We also compiled a list of velocities and positions of galaxies belonging to the three clusters using new data, supplemented with previously measured redshifts available from the literature. Using this data we analyzed the mean velocities and dispersions of the three clusters as well as sub-samples selected based on the X-ray emission. These results were then used to estimate the virial masses of the merging sub-clusters as well as a comparison to the X-ray results.

2.1. ASCA *GIS*

The *ASCA* GIS observations were "cleaned" using standard processing tools (Arnaud 1993) with a conservative version of the filtering criteria (ABC Guide[6]). The data from both GIS detectors was combined in our final analysis, while the SIS detectors, with their smaller field of view, were not used for this study.

To correctly characterize the temperature distribution of these extended sources, a correction for the energy dependent PSF must be applied (Takahashi et al. 1995). We employed a method developed by Churazov and Gilfanov (Churazov et al. 1996, hereafter the CG method), and used previously on other clusters (Donnelly et al. 1998, Donnelly et al. 1999, Churazov et al. 1999, and Henricksen et al. 2000). This method first explicitly corrects the core ($r \leq 6'$) PSF, then approximates the PSF of the wings via a Monte-Carlo simulation. The temperature is then fit in each 15″ pixel using a linear combination of two fiducial single temperature spectra and smoothed at the resolution scale of the telescope ($\sim 5'$) to reduce noise. As shown for A1367 (Donnelly et al. 1998) the results of this method are fully consistent with those found using the method presented by Markevitch et al. (1996 and 1998).

Using this method, we fit a Raymond-Smith model to entirety of each cluster to derive a global gas temperature (T_{ASCA}). The results are given in Table 2. However, the CG method also allowed us to generate two dimensional continuous maps of the gas temperature distributions within the clusters. These temperature maps are shown in Figures 1-3 (top left).

Finally, we also used the CG method to define discrete regions on each cluster and fit the temperature within each region, as shown in Figures 1-3. In each cluster we defined a region around the core of each sub-cluster, two regions to the "outside"– i.e. away from the other sub-component, and a region between the two subclusters. The fit temperatures, with the associated uncertainties, for these regions are shown in the bottom left of Figures 1-3.

2.2. ROSAT *PSPC*

[6]See http://heasarc.gsfc.nasa.gov/docs/asca/abc/abc.html

The *ROSAT* PSPC data were reduced using the standard procedures outlined by Snowden (1994; see also Snowden et al. 1994). By combining only the data from bands 4 through 7 (0.44-2.04 keV), we excluded the lower energies, that generally have higher X-ray background. We chose to not subtract the background at this time, instead opting to include it as an independent component in our fits of the cluster surface brightness described below.

For each of the six sub-clusters in the sample, we generated radial surface brightness profiles in $1'$ annuli centered on the peak emission for each sub-component. The annuli extended from $0'$ to $45'$ and, to minimize contamination of the intensity profile, we excluded the azimuthal half of the profile toward each sub-component's partner. We then measured the average surface brightness (cts s^{-1} $arcmin^{-2}$) in each annulus and fit the resultant surface brightness profile with a standard hydrostatic, isothermal β-model:

$$\Sigma(r) = \Sigma_0 \left[1 + \left(\frac{r}{r_c}\right)^2\right]^{-(3\beta-\frac{1}{2})} \quad (1)$$

(Cavaliere & Fusco-Femiano 1976). The backgrounds were fit by including a constant component in our models. For A1750 and A3395 the backgrounds fell in the range $2.08 - 2.80 \times 10^{-4}$ cts s^{-1} $arcmin^{-2}$, consistent with typical PSPC backgrounds. For both clusters the errors for the two sub-clusters were consistent with single constant backgrounds. A3528 lies near the edge of its *ROSAT* frame (an AGN is actually the target of this observation). We used a nearby region of sky to determine the background and found a count rate of 2.43×10^{-4} cts s^{-1} $arcmin^{-2}$ that was included into our fits for this cluster. The global fit results are given in Table 2.

To search for evidence of a cooling core, we also extracted *ROSAT* spectra from the central $2'$ of each sub-cluster. This small inner core region, where a cooling flow would be most intense, could easily go undetected by *ASCA*'s poorer spatial resolution. Using XSPEC we fit these *ROSAT* spectra with a single temperature (T_{ROSAT}) Raymond-Smith model. The results are given in Table 2. The NE sub-cluster in A1750 and both subclusters in A3528 show central temperatures lower than the overall *ASCA* temperature, indicating the presence of significant cool gas in these sub-clusters. For the SW component of A1750, the fit temperature was consistent with the *ASCA* temperature for the entire cluster, although it has a large uncertainty. For A3395, the *ROSAT* data was unable to constrain the temperature. These results suggest that there are cooling flows in both components of A3528 as well as the NE component of A1750, but not in the SW component of A1750 or either element of A3395.

2.3. *OPTICAL SPECTROSCOPY*

A3395 was observed with the ARGUS fiber spectrograph at the CTIO 4m telescope, and with the Shectograph detector at the 100″ DuPont telescope at the Las Campanas Observatory(LCO). The Shectograph/100″ combination at LCO also was used for all of the spectroscopic observations of A1750. Specifics of the instrumental set ups, observing details, reduction and calibration procedures, as well as an evaluation and discussion of internal and external errors, are given in Quintana & Ramírez (1990). For A3528 the data was drawn from the work by Quintana et al. (2000) on the Shapley Supercluster. The interested reader is directed to that work for a complete discussion of the instrumental configuration.

Velocity determinations were carried out using both a cross-correlation technique and by identifying and fitting line profiles. All reductions were performed using the LONGSLIT, ONEDSPEC and RVSAO packages in IRAF. No systematic internal errors or zero point corrections were found. Typical uncertainties for individual spectra were 30-40 km s^{-1} using the line fitting method. Cross-correlation was applied following the procedures described in Quintana, Ramírez, & Way 1995 (QRW95) using 8 templates. In this case the errors were somewhat higher (40-50 km s^{-1}) compared to the line fitting method. There was no velocity offset between the methods, and the cross-correlation was not applied to spectra with emission lines.

We expect some systematic shifts between velocities for A3395 derived from the two different instrument/telescope configurations (LCO 2.5m and CTIO 4m). We confirmed this on a wider data sample, as discussed in QRW95. Following the discussion there, for the present set, we combined velocities after correcting for a 50 km s^{-1} shift between ARGUS and Shectograph data.

For all three clusters we excluded a small number of objects with obviously discrepant velocities

(i.e. a velocity more than 5,000 km s^{-1} greater or lesser than the peak of the cluster distribution). In the case of A3528 this included 18 objects centered loosely around 23,000 km s^{-1}. These objects are scattered around the field and may represent a background group.

The data for all three clusters also were supplemented by redshifts available through the NASA/IPAC Extragalactic Database (NED). For A3528 four velocities were drawn from Katgert et al. (1998) and the full listing is given in Table 3. No attempt at a determination of a systematic offset was attempted due to the small sample size.

The NED data for A1750 are from Beers et al. (1991) which shares 26 galaxies with our new data (67 galaxies). From a comparison of the velocities of these common objects, we find that our velocities are systematically larger by 69 km s^{-1}. In order to have all of our data in a self-consistent frame, we have applied this offset to the NED data and the offset values are listed in Table 4.

Similarly for A3395, we have 54 Shectograph velocities in common with Teague, Carter & Gray (1990, TCG90) with a systematic offset of 82 kms^{-1}. In the case of the ARGUS data, there are 24 velocities in common with TCG90 and our velocities are larger by 133 kms^{-1}. Both offsets were applied to the NED data and final velocities are listed in Table 5. There are two galaxies observed with ARGUS and published in TCG90 with large discrepant velocities, both with a TCG90 R value below ~2.5, that we included in the cluster redshift, contrary to TCG90 who believe them to be background galaxies.

When galaxies had more than one velocity, we adopted as the final value the weighted mean velocity and the associated uncertainty. Weighting factors came from the published uncertainties combined with our internal uncertainties. More details about this procedure are extensively discussed in QRW95.

Using the statistical prescriptions described in Beers et al. (1990) we determined the "mean" velocity for each of our three clusters (see Table 2). We find generally excellent agreement with previous results (Abell, Corwin, & Olowin 1989, Struble & Rood 1999). One exception is that for A3528. Our results give a "mean" velocity more than 500 km s^{-1} larger than that found by Struble & Rood (1999), but which is more consistent with the values found previously for this cluster by Abell, Corwin, & Olowin (1989) and Katgert et al. (1996).

The positions of the galaxies are shown with the X-ray intensity isophotes from *ROSAT* overlaid in Figures 1-3. We expanded the field of view from that shown for the temperature maps to include all of the galaxies that appear to be members of each cluster. Galaxies with lower velocities than our "mean" cluster velocity are shown in blue while those with higher velocities are shown in red. A velocity histogram for each cluster is also presented.

We note that A3395 has a high velocity bump in its distribution. These objects are shown in Figure 3 as open circles. While they are localized in velocity space, they are distributed very widely across the field of view. This suggests that it is unlikely that they are a background group, and thus they have simply been bundled into the overall sample.

3. RESULTS AND ANALYSIS

3.1. *MASSES*

We first estimated the mass of the X-ray emitting gas by using the luminosities for the subclusters determined from the *ROSAT* data and solving for the central density,

$$L(r) = \frac{2\pi n_e n_H \Lambda_0 a^3}{(1-3\beta)} \times \int_0^\infty \left[\left(1 + s^2 + \left[\frac{r}{a}\right]^2\right)^{-3\beta+1} - (1+s)^{-3\beta+1} \right] ds \quad (2)$$

(David et al. (1990). The gas density distribution is then integrated to the radius of interest,

$$M_{gas}(r) = 4\pi\rho_0 \int_0^r \left[1 + \left(\frac{s}{r_c}\right)^2\right]^{-\frac{3\beta}{2}} ds \quad (3)$$

Gas masses within 0.5 and 1.0 Mpc are given in Table 6.

We estimated the total mass of each sub-cluster assuming spherical symmetry, hydrostatic equilibrium and using our fit values for the core radii and β's. With these assumptions the mass contained within a radius r is,

$$M(<r) = -\frac{kT(r)}{\mu m_p G}\left(\frac{d\log\rho_g(r)}{d\log r} + \frac{d\log T(r)}{d\log r}\right) r. \quad (4)$$

Markevitch et al. (1998, 1999) found that the temperature profiles of galaxy clusters are well approximated by a polytropic equation of the form,

$$T \propto (1 + r^2)^{-\frac{3}{2}\beta(\gamma-1)} \quad (5)$$

where $\gamma \simeq 1.24$. Using this function for the temperature, Equation 4 reduces to

$$M(r) = 3.70 \times 10^{13} M_{\odot} \frac{0.60}{\mu} T(r) r \frac{3\beta\gamma r^2}{r_c^2 + r^2}, \quad (6)$$

where $T(r)$– derived from the fit temperature in the core of each sub-cluster– and r are measured in keV and Mpc respectively.

Although the presence of a merger and the subsequent heating of the ICM gas introduces uncertainties in the estimates of both the gas and total masses, these estimates do provide a means of comparing the relative masses of the subclusters. The results are given in Table 6.

The cluster velocity distributions also demonstrate typical dispersions with scales of order 1000 km s^{-1}. Using only galaxies with projected distances from a subcluster core of 0.5 Mpc or less and again employing the statistical methods of Beers et al. (1990), we examined the characteristics of velocity distributions of each core. Table 6 gives the virial masses which we find to be in good agreement with the results from our X-ray analysis. Table 7 gives the details of the velocity distributions and is consistent with typical sub-cluster sized masses.

Two circles indicate the radial extent of the two different subcluster core elements the surface distribution maps of the galaxies in Figures 1, 2 and 3. The velocity histograms of the two core samples in each cluster have been color coded to the circles and shown along with the overall velocity histograms. For A3395 the two cores are in such close proximity that the 0.5 Mpc circles overlap and there are nine objects in common. The measured scales reported in Table 7 for the two subsamples in A3395 were performed both including and excluding the disputed objects. These disputed objects were excluded from the sub-clump velocity histograms with the number of disputed galaxies in each bin indicated above that bin.

Following the approach outlined by Beers, Geller and Huchra (1982), we estimated the virial mass of each sub-cluster. Assuming that they are bound and the velocity dispersions are isotropic, the total mass of each sub-cluster is

$$M_{virial} = \frac{3\pi}{G} \sigma_r^2 \left\langle \frac{1}{r_p} \right\rangle^{-1}, \quad (7)$$

where σ_r is the velocity dispersion along the line of sight and $\left\langle \frac{1}{r_p} \right\rangle^{-1}$ is the harmonic mean projected separation on the sky. The masses and values for $\left\langle \frac{1}{r_p} \right\rangle^{-1}$ are given in Table 6. All of the virial masses, except for the southeast element of A3528, are in good agreement with those determined from the X-ray data.

For the southeast clump of A3528, whose optically determined virial mass is twice the X-ray derived mass, we note that the velocity distribution for this sub-clump has a very extended tail with two galaxies having rather large relative velocities (δV = 1069 and 1554km s^{-1}) compared to the mean sub-clump velocity. If these two galaxies are excluded from the velocity calculations for the southeastern clump, the dispersion drops from 930 km s^{-1} to 513 km s^{-1}. While the average projected distance increases slightly with this exclusion, the overall effect is to reduce the estimated virial mass by a factor of three, which brings it into agreement with all of the other mass estimates.

4. DISCUSSION

Our data suggest that these three clusters represent progressive stages of first time merger events prior to first core passage. A3528, with its very azimuthally symmetric intensity isophotes appears to be at the earliest stage, when gas in the outer halos of the sub-clumps is just beginning to interact. In A1750, the effects of the merger have begun to distort the intensity isophotes, while A3395 with its clearly disrupted intensity distribution appears to be nearly at first core passage.

Other than their merger state, all three clusters appear to be generally normal. They all have gas fractions of $\sim 20\%$ at 0.5 and $\sim 30\%$ at 1.0 Mpc, and their fit β values and core radii (Table 2) are typical for galaxy clusters (Jones & Forman 1984, Jones & Forman 1999, and Vikhlinin et al. 1999).

All three temperature maps have elevated gas temperatures in the region between the two emission peaks. For all three, the deviation from the overall mean temperature is significant at the 90% confidence level. In A3528 the deviation between the merger region (region 3 for all three clusters)

and the other regions is the least pronounced and could still be consistent with a uniform temperature throughout the entire cluster– excepting the far northeastern side where the temperature is especially low.

We find a similar result for the temperature data from A1750. In this case however the temperature of the merger region also is inconsistent with the temperature of the southwestern core. This suggests that a shock region is developing in the gas, as it is compressed between the two sub-clusters.

Finally, A3395 clearly demonstrates the compression and concomitant heating of the gas that would be expected in events similar to that modeled by Roettiger, Burns & Loken (1996; see also Roettiger, Loken & Burns 1997) and Norman & Bryan (1999).

The *ROSAT* data indicates that cool gas is still present in both of the subcluster cores in A3528. In A1750 we find emission from cool gas, but while the fit temperature for the northeastern clump is reasonably well determined, the solution for the southwestern core is high and marginally constrained at best. In contrast the fit temperatures for both cores in A3395 were completely unconstrained indicating that little if any cool gas remains. Thus as the merging process occurs, we appear to be observing the disruption of the cooling flow.

We modeled the overall dynamics of the merging systems. To do this we assumed that the two sub-clumps are falling towards each other on linear orbits, i.e. that there is no net rotation to the system as a whole, and that they can be treated as point masses. Following the treatment developed by Beers, Geller and Huchra (1982), we present plots of relative radial velocity (V_r) versus projection angle from the plane of the sky(α) for all three clusters in Figure 4.

In the plots the dashed curves separate states which are bound from those which are unbound, as determined by simple Newtonian gravitational energy considerations. A bound state must fulfill the condition

$$V_r^2 R_p \leq 2GM \sin^2\alpha \cos\alpha, \tag{8}$$

where R_p is the projected separation of the two sub-clusters, and M is the sum of the masses of the two sub-clumps (i.e. the entire system).

The allowed bound solutions for a linear orbit must fulfill the following parametric equations of motion for physical separation, time and relative velocity:

$$R = \frac{R_m}{2}(1 - \cos\chi), \tag{9a}$$

$$t = \left(\frac{R_m^3}{8GM}\right)^{\frac{1}{2}} (\chi - \sin\chi), \tag{9b}$$

$$V = \left(\frac{2GM}{R_m}\right)^{\frac{1}{2}} \frac{\sin\chi}{(1 - \cos\chi)}, \tag{9c}$$

where R_m is the maximum separation of the two sub-clusters, M is the mass of the entire system and χ is the parametric variable.

A similar set of equations is valid for the unbound solutions:

$$R = \frac{GM}{V_\infty^2}(\cosh\chi - 1), \tag{10a}$$

$$t = \frac{GM}{V_\infty^3}(\sinh\chi - \chi), \tag{10b}$$

$$V = V_\infty \frac{\sinh\chi}{(\cosh\chi - 1)}, \tag{10c}$$

where V_∞ is the asymptotic expansion velocity. As did Fabricant et al. (1994), we note the correction of the exponent on V_∞ in Equation 10a from that presented in Beers, Geller and Huchra (1982).

In both systems of equations, the observables V_r and R_p are related to the system variables by,

$$V_r = V \sin\alpha, \text{ and } R_p = R\cos\alpha. \tag{11}$$

The relative velocities are given in Table 7, and the projected separations are 0.93, 1.00 and 0.67 Mpc for A3528, A1750 and A3395 respectively. The systems of equations are closed by setting t to be the age of the universe: within our chosen cosmology $t_o = 3.16 \times 10^{17}$ s.

In Figure 4 the allowed linear solutions are shown as solid lines, with the bound solutions to the left of the Newtonian binding condition line and the unbound to the right. We added our measurement of the relative velocity as a solid vertical line with a one sigma confidence region marked by

cross-hashings. We note that the bound solutions with values of α greater than the inflection point are out-bound, while the others are in-bound.

From Figure 4 we can see that every reasonable configuration for both A3528 and A3395 indicates that the systems are bound. However, this analysis suggests that the A1750 system is *not* bound. This is in contrast to similar previous work on this cluster by Beers et al. (1991). While our mass for this cluster is only slightly smaller than their "doubled" mass simulation (6.1 vs 6.8 $\times 10^{14}$ $M_\odot$), the larger R_p, implied by our cosmology, and the increase in V_r, from our improved velocity sample, make a linear bound orbit relatively unlikely. However, we also modeled the system with the mass increased by 50% to account for the other nearby mass concentrations (Beers et al. 1991, Einasto et al. 1997, Jones & Forman 1999). This is presented in Figure 4 and shows that it is now quite likely that the system is bound, even for the assumption of a simplified linear orbit.

5. SUMMARY

Using data from *ROSAT* and *ASCA* we developed temperature and density distributions for the hot X-ray emitting gas in three binary galaxy clusters: A3528, 1750 and 3395.

We find that the surface brightness distribution for each sub-clusters separately within each binary are generally consistent with other single clusters. The values for β and R_c, as well as the luminosities, are typical. This is somewhat remarkable in that the intensity isophotes of all three binaries show various amounts of distortion, suggesting early stages of merging.

Using new velocity data, supplemented with measurements from the literature for each cluster, we generated estimates of the mean velocities for the sub-clusters as well as for the overall cluster, estimates of the dispersions (the "scale" of the distributions) and velocity histograms. Two of the clusters (A3528 and A3395) show no significant differences in the velocities of the subclusters and thus the in-fall appears to be nearly in the plane of the sky. For A1750 the velocity difference of the subclusters is 1335 km s^{-1}, suggesting that the merger lies more along the line of sight.

Our estimates of the mass using the X-ray luminosity, the fit surface brightness profile and the virial method are self consistent and typical of the values found for single clusters.

We also produced an analysis of their orbital dynamics assuming a simple linear model and find that A3528 and A3395 are nearly certainly bound to each other, as is A1750 (after including mass from other nearby elements).

The temperature results indicate some heating of the intra-cluster gas, consistent with the level of disruption of the surface brightness distributions. The most prominent feature is the heating of the gas located between the subclusters of each binary. In addition, the absence of cool gas in the cores of three of the subclusters (both parts of A3395 and the southwest element of A1750) may have resulted from the disruption of the fooling flow by the merger.

Our observations suggest that A3528 is in the extreme early stages of a merger. Although bound to each other, the gas in both sub-clusters is only just beginning to interact. Both cores show evidence of cool gas, and the intensity contours are still azimuthally symmetric. At the same time the gas located between the subclusters has been heated 14% above the average cluster temperature due to the effects of the impending collision.

A1750 is slightly further along in the merging process. One of the sub-clusters retains its cool gas in the core, but the other most likely does not. There is some elongation of the intensity isophotes and the gas between the cores shows significant (28% above the average) heating.

Finally, A3395 is nearly at first core passage. Neither core shows evidence for cool gas, the intensity isophotes are highly disrupted and the temperature distribution clearly shows strongly heated gas (30% above the overall average) between the two sub-clusters.

Taken together these three binary clusters present a sequence of views of a typical merger event in a galaxy cluster. More detailed spectroscopic studies with *CHANDRA* and *XMM* will further provide details of the merging process and its effects its effects on both the intra-cluster medium and the resident galaxies.

TABLE 1
OBSERVATIONAL DATA

Cluster	α (J2000)	δ (J2000)	ROSAT			ASCA		
			Sequence #	Date	Live Time (ksec)	Sequence #	Date	On Tim (ksec)
A3528	12:54:29	-29:07:00	300093	7/16/96	15.0	84057000	1/15/96	18.9
A1750	13:31:00	-1:47:18	800553	7/01/93	12.7	81010000	1/27/94	33.5
A3395	6:27:03	-54:08:48	800079	7/16/91	2.6	82033000	2/14/95	31.1

TABLE 2
INTENSITY AND TEMPERATURE FITS

Cluster	z	T_{ASCA} (keV)	β	r_c (Mpc)	T_{ROSAT} (keV)
A3528 SE	0.0545	4.7 ± 0.3	$0.55^{+0.02}_{-0.01}$	$0.14^{+0.02}_{-0.02}$	$2.1^{+0.7}_{-0.4}$
A3528 NW			$0.59^{+0.04}_{-0.04}$	$0.14^{+0.03}_{-0.02}$	$2.3^{+1.3}_{-0.5}$
A1750 NE	0.0855	3.6 ± 0.2	$0.52^{+0.04}_{-0.03}$	$0.17^{+0.04}_{-0.02}$	$1.9^{+1.3}_{-0.5}$
A1750 SW			$0.65^{+0.04}_{-0.04}$	$0.23^{+0.04}_{-0.02}$	$4.2^{+3.5}_{-1.7}$
A3395 NE	0.0506	4.5 ± 0.2	$0.66^{+0.26}_{-0.13}$	$0.32^{+0.18}_{-0.11}$	NC [a]
A3395 SW			$0.60^{+0.23}_{-0.12}$	$0.28^{+0.18}_{-0.11}$	

[a]This fit was not constrained.

TABLE 3
ABELL 3528 VELOCITIES

α (J2000)	δ (J2000)	v (km s^{-1})	Reference	α (J2000)	δ (J2000)	v (km s^{-1})	Reference
12:52:37.8	-28:54:47	16052 ± 50	1	12:54:35.7	-29:06:38	16254 ± 60	1
12:53:15.9	-29:19:04	16403 ± 50	1	12:54:38.4	-28:58:56	17101 ± 50	1
12:53:26.1	-28:54:11	16336 ± 61	1	12:54:39.8	-28:56:32	15759 ± 51	1
12:53:31.2	-29:27:18	15201 ± 61	1	12:54:39.8	-29:27:33	15045 ± 59	1
12:53:40.6	-28:48:58	16633 ± 132	1	12:54:40.5	-29:01:49	15827 ± 50	2,3
12:53:45.6	-29:02:53	14872 ± 48	2	12:54:41.0	-28:53:00	16432 ± 50	1
12:53:52.0	-28:36:15	14791 ± 50	1	12:54:41.0	-29:13:37	16783 ± 123	1
12:53:54.6	-28:34:04	14671 ± 50	1	12:54:42.5	-29:01:00	22737 ± 50	1
12:53:58.2	-29:31:09	17631 ± 52	1	12:54:43.1	-28:52:16	16237 ± 50	1
12:54:00.8	-28:44:07	16680 ± 50	1	12:54:48.6	-29:12:00	15824 ± 79	1
12:54:01.6	-28:30:00	16528 ± 50	1	12:54:49.2	-29:09:54	17260 ± 70	1
12:54:03.9	-29:04:22	17303 ± 50	1	12:54:50.7	-28:41:47	14560 ± 50	1
12:54:10.6	-29:10:41	17177 ± 50	1	12:54:52.2	-29:16:16	14486 ± 50	1
12:54:11.3	-29:01:46	16622 ± 50	1	12:54:52.4	-28:43:17	16986 ± 73	1
12:54:12.1	-29:09:22	15894 ± 50	1	12:54:53.2	-28:31:58	15426 ± 50	1
12:54:14.3	-28:59:16	16784 ± 50	1	12:54:53.9	-29:00:46	16174 ± 70	1
12:54:15.6	-29:00:19	15437 ± 86	1	12:54:55.3	-29:30:11	16329 ± 137	1
12:54:16.3	-28:45:23	15548 ± 50	1	12:54:56.2	-28:55:40	15926 ± 50	1
12:54:16.9	-29:01:16	15119 ± 50	1	12:54:56.4	-29:06:28	13816 ± 100	1
12:54:17.6	-29:00:47	16186 ± 113	1	12:55:04.3	-29:15:56	17007 ± 57	2
12:54:18.9	-29:18:11	16083 ± 54	2	12:55:18.6	-29:12:04	16866 ± 68	1
12:54:20.5	-29:04:10	16287 ± 50	1	12:55:19.7	-29:17:20	16476 ± 54	2
12:54:21.5	-29:13:23	16834 ± 50	1	12:55:21.0	-28:57:01	15834 ± 65	1
12:54:22.2	-29:00:45	16219 ± 50	1	12:55:27.6	-28:47:50	17487 ± 51	1
12:54:22.9	-29:04:17	17391 ± 71	1	12:55:29.6	-28:45:35	17367 ± 109	1
12:54:23.3	-29:01:05	16353 ± 63	3	12:55:33.0	-28:48:52	17740 ± 69	1
12:54:23.5	-29:10:02	16530 ± 50	1	12:55:40.2	-28:34:33	17073 ± 50	1
12:54:24.7	-28:59:36	16914 ± 50	1	12:55:43.6	-29:24:41	18479 ± 94	1
12:54:25.3	-28:58:24	14664 ± 50	1	12:55:44.8	-29:01:11	16810 ± 50	1
12:54:26.7	-28:57:20	15720 ± 50	1	12:55:50.8	-28:45:16	16298 ± 50	1
12:54:28.1	-28:57:42	14122 ± 50	1	12:55:57.5	-29:17:58	16757 ± 57	1
12:54:28.1	-29:00:42	13413 ± 260	1	12:56:13.0	-29:13:44	16825 ± 118	1
12:54:28.8	-29:17:31	14971 ± 63	1	12:56:20.9	-28:59:14	17885 ± 54	1
12:54:31.5	-28:55:18	16790 ± 50	1	12:56:24.9	-29:12:59	16963 ± 50	1
12:54:35.3	-29:04:41	16217 ± 55	1	12:56:27.6	-29:08:54	17825 ± 79	1
12:54:35.4	-29:00:39	14713 ± 50	1	12:56:27.9	-29:08:55	17719 ± 50	1

REFERENCES.— (1)Quintana et al. 2000; (2)Katgert et al. 1998 ; (3)Quintana et al. 1995

TABLE 4
ABELL 1750 VELOCITIES

α (J2000)	δ (J2000)	v (km s^{-1})	Reference	α (J2000)	δ (J2000)	v (km s^{-1})	Reference
13:30:15.2	-1:31:09	27131 ± 28	1	13:30:57.4	-1:44:31	22939 ± 20	1,2
13:30:18.4	-2:00:48	26145 ± 23	1,2	13:30:58.2	-1:51:13	25413 ± 50	1
13:30:18.7	-1:32:44	24826 ± 22	1	13:30:59.8	-1:43:36	24780 ± 40	1,2
13:30:32.3	-1:47:36	26297 ± 28	1	13:31:01.2	-1:50:52	26012 ± 30	1,2
13:30:32.9	-1:39:35	25171 ± 35	1	13:31:04.7	-1:38:04	24665 ± 33	1
13:30:34.4	-1:47:45	25034 ± 34	1	13:31:06.1	-1:40:48	25184 ± 30	1,2
13:30:34.5	-1:48:27	26354 ± 100	2	13:31:06.4	-1:44:14	24400 ± 50	2
13:30:35.1	-1:49:05	24543 ± 36	1	13:31:09.7	-1:44:45	25229 ± 50	2
13:30:36.8	-1:53:04	25951 ± 23	1,2	13:31:09.9	-1:41:09	24510 ± 20	1,2
13:30:38.2	-1:50:36	25598 ± 24	1,2	13:31:10.4	-1:38:03	25880 ± 37	1
13:30:48.9	-1:53:56	27585 ± 46	1,2	13:31:10.8	-1:43:49	25019 ± 41	1,2
13:30:41.4	-1:41:14	26165 ± 44	1	13:31:11.0	-1:43:41	25058 ± 26	1,2
13:30:42.5	-1:51:24	25247 ± 26	1,2	13:31:11.2	-1:43:35	25381 ± 24	1,2
13:30:44.4	-1:53:19	26408 ± 23	1,2	13:31:13.3	-1:58:42	26903 ± 38	1
13:30:44.5	-1:59:29	24809 ± 30	1	13:31:13.9	-1:48:58	25740 ± 38	1
13:30:45.5	-1:48:43	24051 ± 57	2	13:31:14.7	-1:30:17	25461 ± 37	1
13:30:46.1	-1:52:28	26434 ± 31	1,2	13:31:16.2	-1:59:35	27684 ± 43	1
13:30:48.1	-1:52:02	26231 ± 32	1,2	13:31:19.3	-1:42:19	24339 ± 50	2
13:30:48.1	-1:52:12	25118 ± 25	1,2	13:31:19.5	-1:45:39	24522 ± 27	1,2
13:30:48.5	-1:37:48	25100 ± 42	1	13:31:22.2	-1:43:14	24933 ± 50	2
13:30:49.0	-1:52:52	27926 ± 50	2	13:31:23.1	-2:01:37	26731 ± 45	1
13:30:49.1	-1:53:56	27361 ± 50	2	13:31:23.4	-1:43:35	22724 ± 23	1,2
13:30:49.8	-1:40:40	24328 ± 20	1	13:31:23.9	-1:53:35	26343 ± 37	1
13:30:50.1	-1:47:55	26260 ± 30	1,2	13:31:27.9	-1:43:50	25260 ± 41	2
13:30:50.4	-1:51:27	26086 ± 24	1,2	13:31:30.0	-1:39:25	25259 ± 24	1,2
13:30:50.5	-1:51:44	26472 ± 29	1,2	13:31:36.6	-1:40:08	24623 ± 43	2
13:30:50.8	-1:51:37	26088 ± 26	1,2	13:31:37.7	-1:52:25	26268 ± 39	1
13:30:53.0	-1:37:31	24965 ± 30	1	13:31:49.5	-1:58:52	26610 ± 31	1
13:30:54.2	-1:52:33	26512 ± 31	1,2	13:31:50.1	-1:57:38	27081 ± 30	1
13:30:55.6	-1:55:13	23632 ± 43	1	13:31:50.9	-1:41:15	24889 ± 35	1
13:30:56.3	-1:54:08	26873 ± 50	2	13:31:52.1	-1:56:07	26789 ± 28	1
13:30:56.4	-1:42:20	27244 ± 50	2	13:31:54.4	-1:43:44	25915 ± 21	1
13:30:56.6	-1:43:24	24704 ± 23	1,2	13:31:56.7	-1:49:35	22697 ± 44	1
13:30:56.7	-1:53:58	25515 ± 29	1,2	13:32:15.5	-1:43:13	26803 ± 22	1

REFERENCES.— (1) LCO-SHECTOGRAPH; (2)Beers et al. 1991

TABLE 5
ABELL 3395 VELOCITIES

α (J2000)	δ (J2000)	v (km s^{-1})	Reference	α (J2000)	δ (J2000)	v (km s^{-1})	Reference
6:24:23.2	-54:29:48	14478 ± 105	1	6:27:23.7	-54:28:23	15743 ± 70	1,2
6:24:26.9	-54:32:55	15741 ± 71	1	6:27:24.4	-54:26:30	14440 ± 32	2
6:24:30.1	-54:07:36	15338 ± 69	1	6:27:26.6	-54:25:48	15099 ± 30	1,2
6:24:32.2	-54:10:04	14012 ± 49	1	6:27:26.3	-54:31:02	15735 ± 42	1,4,7
6:24:35.6	-54:07:47	14324 ± 48	1	6:27:29.8	-54:27:19	15024 ± 52	1,4
6:24:38.8	-54:14:18	14410 ± 101	1	6:27:30.5	-54:35:48	17949 ± 39	1,2
6:24:48.9	-54:14:48	13808 ± 242	1,2,3	6:27:36.1	-54:24:05	14675 ± 72	1
6:24:60.0	-54:10:31	17463 ± 30	1,2	6:27:36.3	-54:26:58	14562 ± 30	1,2,5,7
6:25:04.0	-54:22:21	13835 ± 91	1,2	6:27:35.6	-54:40:04	16106 ± 77	1
6:25:04.8	-54:09:41	17625 ± 110	1	6:27:38.2	-54:25:50	16486 ± 118	1
6:25:09.3	-54:25:01	17570 ± 44	1,2	6:27:39.1	-54:22:38	13754 ± 925	1,4
6:25:15.3	-54:16:15	17670 ± 276	1,2	6:27:39.4	-54:27:43	14676 ± 30	1,2
6:25:20.1	-54:21:36	14502 ± 108	1	6:27:40.0	-54:26:55	16222 ± 34	2
6:25:22.4	-54:16:54	17504 ± 57	1,4	6:27:41.0	-54:27:15	17046 ± 71	1,4,5
6:25:31.5	-54:34:41	15088 ± 105	1	6:27:41.3	-54:23:48	16553 ± 131	1
6:25:48.3	-54:11:43	14293 ± 82	1,4	6:27:40.5	-54:36:50	15676 ± 47	1
6:25:49.1	-53:59:36	13910 ± 89	1,5	6:27:41.9	-54:17:25	14342 ± 78	1
6:25:47.8	-54:39:53	16401 ± 76	1	6:27:40.9	-54:35:34	15465 ± 170	1,3
6:25:51.2	-54:18:22	16134 ± 88	1	6:27:42.0	-54:32:19	15245 ± 163	1,2
6:25:57.0	-54:27:50	18047 ± 91	1,3,4	6:27:44.3	-54:07:10	14912 ± 163	1,2
6:25:58.4	-54:27:44	18263 ± 35	2	6:27:44.2	-54:16:51	16158 ± 83	1
6:26:01.0	-54:27:40	18153 ± 139	1	6:27:43.8	-54:24:26	13712 ± 33	1,2
6:26:08.7	-54:22:04	14777 ± 92	1	6:27:43.7	-54:27:19	16248 ± 73	1,4,5
6:26:07.9	-54:40:30	15499 ± 79	1,2,6	6:27:44.6	-54:26:45	13265 ± 84	1,2,5
6:26:10.3	-54:27:24	15670 ± 43	1,2	6:27:47.0	-54:25:10	16305 ± 201	1,3,4
6:26:10.4	-54:32:26	16418 ± 56	1,2	6:27:47.6	-54:25:28	14872 ± 52	1
6:26:11.5	-54:17:14	14960 ± 33	4	6:27:49.1	-54:04:03	17986 ± 41	2
6:26:12.0	-54:17:08	15224 ± 42	2	6:27:48.6	-54:32:19	13076 ± 55	4
6:26:12.1	-54:23:40	14230 ± 106	1	6:27:50.9	-54:09:05	14586 ± 69	1
6:26:11.4	-54:40:16	17627 ± 98	1	6:27:51.1	-54:09:07	14926 ± 223	1,2
6:26:13.7	-54:24:19	17728 ± 30	1,2	6:27:50.7	-54:28:22	15535 ± 55	1,2
6:26:15.2	-54:19:37	14659 ± 75	1	6:27:52.5	-54:30:04	14322 ± 311	1,4
6:26:16.8	-54:20:17	14911 ± 31	1,2	6:27:52.1	-54:36:52	16616 ± 104	1
6:26:17.3	-54:32:26	15887 ± 81	1,2	6:27:54.5	-54:31:24	16152 ± 166	1,2
6:26:20.7	-54:15:32	14543 ± 112	1,2,3	6:27:56.3	-54:26:02	13983 ± 66	4
6:26:24.1	-54:20:38	14755 ± 77	1,2	6:27:58.5	-54:32:50	16143 ± 188	1
6:26:27.4	-54:28:35	14797 ± 98	1	6:27:59.3	-54:29:44	15097 ± 104	1,2
6:26:30.5	-54:17:57	13248 ± 81	1	6:28:01.4	-54:35:09	15360 ± 94	1
6:26:31.5	-54:36:55	14172 ± 50	2	6:28:02.0	-54:34:14	14153 ± 89	1,2
6:26:32.4	-54:34:01	16305 ± 30	2	6:28:05.8	-54:24:12	15033 ± 35	1
6:26:34.3	-54:10:00	13544 ± 78	1,2	6:28:08.0	-54:34:18	15530 ± 76	1,2
6:26:34.7	-54:09:50	14621 ± 35	2	6:28:13.2	-54:15:35	16437 ± 39	1,2
6:26:34.5	-54:21:25	15264 ± 202	1,3,4	6:28:12.5	-54:29:47	16163 ± 48	2
6:26:34.6	-54:25:56	15548 ± 69	1	6:28:15.2	-54:35:23	15793 ± 134	1,2,7
6:26:35.8	-54:29:31	15853 ± 51	1,3,4	6:28:16.6	-54:31:39	15909 ± 74	1,2,7

RHD, WF, CJ acknowledge support from the Smithsonian Institute and NASA contract NAS8-39073. HQ acknowledges partial support from FONDECYT grant 8970009 and the award of a Presidential Chair in Science (Chile).

REFERENCES

Abell, G.O., Corwin, H.G. & Olowin, R.P. 1989, ApJS, 70, 1.

Arnaud, K. 1993, *ASCA* Newsletter, No. 1 (NASA/GSFC).

Beers, T.C., Geller, M.J. & Huchra, J.P. 1982, ApJ, 257, 23.

Beers, T.C., Flynn, K., & Gebhardt, K. 1990, AJ, 100, 32.

Beers, T., Forman, W., Huchra, J., Jones, C. & Gebhardt, K. 1991, AJ, 102, 1581

Bird, C. M. 1994, AJ, 107, 1637.

Cavaliere, A. & Fusco-Femiano, R. 1976, A&A, 49, 137.

Churazov, E., Gilfanov, M., Forman, W. & Jones, C. 1996, ApJ, 471, 673

Churazov, E., Gilfanov, M., Forman, W. & Jones, C. 1999, ApJ, 520, 105

David, L.P., Arnaud, K.A., Forman, W. & Jones, C. 1990, ApJ, 356, 32

Donnelly, R. Hank, Markevitch, M., Forman, W., Jones, C., Churazov, E. & Gilfanov, M. 1999, ApJ, 513, 690.

Donnelly, R. Hank, Markevitch, M., Forman, W., Jones, C., David, L.P., Churazov, E. & Gilfanov, M. 1998, ApJ, 500, 138.

Dressler, A. & Shectman, S. A. 1988, AJ, 985.

Einasto, M., Tago, E., Jaaniste, J., Einasto, J., & Andernach, H. 1997, A&AS, 123, 119.

Evrard, A. E. 1990a, ApJ, 363, 349.

Evrard, A. E. 1990b, in Clusters of Galaxies, eds. Oegerle, Fitchett and Danly (Cambridge: Cambridge University Press), 287.

Fabricant, D.G., Bautz, M.W. & McClintock, J.E. 1994, AJ, 107, 8.

Forman, C. & Jones, C. 1990, in Clusters of Galaxies, ed. W. Oergerle, M. Fitchett, & L. Danly (Cambridge: Cambridge Univ. Press), 257.

Forman, W., Bechtold, J., Blair, W., Giacconni, R., Van Speybroeck, L., & Jones, C. 1981, ApJL, 243, L133.

Geller, M.J., & Beers, T.C. 1982, PASP, 94, 421.

Henricksen, M., Donnelly, R. Hank & Davis, D. 2000, ApJ, 529, 692.

Henriksen, M. & Markevitch, M. 1996, ApJL, 466, L79.

Henry, J.P. & Briel, U.G. 1995, ApJL, 443, L9.

Hopp, U. and Materne, J. 1985, A&A, 148, 359

Jones, C. & Forman, W.R. 1999, ApJ, 511, 65.

Jones, C. & Forman, W.R. 1984, ApJ, 276, 38.

Katgert, P., Mazure, A., Perea, J., den Hartog, R., Moles, M., Le Fevre, O., Dubath, P., Focardi, P., Rhee, G., Jones, B., Escalera, E., Biviano, A., Gerbal, D. & Giuricin, G. 1996, A&A, 310,8.

Katgert, P., Mazure, A., den Hartog, R., Adami, C., Biviano, A., and Perea, J. 1998, A&AS, 129, 399.

Maddox, S.J., Efstathiou, G., Sutherland, W.J. and Loveday, J. 1990, MNRAS, 243, 692.

Markevitch, M., Ponman, T. J., Nulsen, P.E.J., Bautz, M.W., Burke, D.J., David, L.P., Davis, D., Donnelly, R.H., Forman, W.R., Jones, C., Kaastra, J., Kellogg, E., Kim, D.-W., Kolodziejczak, J., Mazzotta, P., Pagliaro, A., Patel, S., Van Speybroeck, L., Vikhlinin, A., Vrtilek, J., Wise, M. & Zhao, P. 2000, ApJ, 541, 542.

Markevitch, M., Vikhlinin, A., Forman, W.R & Sarazin, C.L. 1999, ApJ, 527, 545.

Markevitch, M., Forman, W.R., Sarazin, C.L. & Vikhlinin, A. 1998, ApJ 503, 77.

Markevitch, M., Sarazin, C. & Irwin, J.A. 1996a, ApJ, 472, L17.

Markevitch, M., Mushotzky, R., Inoue, H., Yamashita, K., Furuzawa, A., & Tawara, Y. 1996b, ApJ, 456, 437

Materne, J., Chincarini, G., Tarenghi, M. & Hopp, U. 1982, A&A, 109, 238

Mohr, J., Fabricant, D.G., Geller, M. J., and Evrard, A.E. 1995, ApJ, 447, 8.

Norman, M.L. & Bryan, G.L. 1999, in "The Radio Galaxy Messier 87", ed. Röser, H.-J. & Meisenheimer, K. (New York, Springer), p. 106

Quintana H., Ramírez A., 1990, AJ, 100, 1424.

Quintana H., Ramírez, A., Melnick, J., Raychaudhury, S., & Slezak, E. 1995, AJ, 110, 463.

Quintana H., Ramírez, A., & Way M.J. 1996, AJ, 112, 36.

Quintana H., Carrasco, E.R., & Reisenegger, A. 2000, AJ, 120, 511.

Raychaudury, S., Fabian, A.C., Edge, A.C., Jones, C. & Forman, W. 1991, MNRAS, 248, 101.

Richstone, Loeb & Turner 1992, ApJ, 393, 477.

Ricker, P.M. 1998, ApJ , 496, 670.

Roettiger, K., Burns, J.O., & Loken, C. 1996, ApJ, 473, 651.

Roettiger, K., Loken, C. & Burns, J.O. 1997, ApJS, 109, 307.

Schindler, S., & Müller, E. 1993, A&A, 272, 137.

Slezak, E., Durret, F. & Gerbal, D. 1994, AJ, 108, 1996.

Snowden, S.L. 1994, Cookbook for Analysis Procedures for *ROSAT* XRT/PSPC Observations of Extended Objects and the Diffuse Background.

Snowden, S.L., McCammon, D., Burrows, D.N. & Mendenthall, J.A. 1994, ApJ, 424, 714.

Struble, M.F. & Rood, H.J. 1999, ApJS, 125, 35.

Takahashi, T., Markevitch, M., Fukuzawa, Y., Ikebe, Y., Ishiaki, Y., Kikuchi, K., Makishimi, K. & Tarawa, Y. 1995, *ASCA* Newsletter, No. 3 (NASA/GSFC).

Teague, P.F., Carter, D. & Gray, P. 1990, ApJS, 72, 715

Vidal, N.V. 1975 PASP, 87, 625

Vikhlinin, A., Forman, W. & Jones, C. 1999, ApJ, 525, 47.

West and Frandsen 1981, A&AS, 44, 329

White, D.A., Jones, C. & Forman, W. 1997, MNRAS, 292, 419.

White, D.A. 1999 *private communication.*

TABLE 5—*Continued*

α (J2000)	δ (J2000)	v (km s^{-1})	Reference	α (J2000)	δ (J2000)	v (km s^{-1})	Reference
6:26:37.5	-54:26:02	14542 ± 150	1,4	6:28:18.7	-54:15:09	15686 ± 99	1,3,4
6:26:40.1	-54:12:03	15623 ± 81	1	6:28:18.9	-54:21:36	14548 ± 72	1
6:26:40.2	-54:11:23	17655 ± 115	1	6:28:20.3	-54:36:38	14983 ± 153	1,2
6:26:40.0	-54:20:02	14139 ± 30	1,2	6:28:21.2	-54:25:25	15451 ± 238	1,2
6:26:40.4	-54:32:48	18213 ± 49	2	6:28:23.1	-54:20:00	14591 ± 102	1
6:26:43.4	-54:19:14	14675 ± 896	1,2	6:28:23.2	-54:35:55	15432 ± 47	1,2
6:26:43.5	-54:26:16	15500 ± 116	1	6:28:29.1	-54:22:48	14685 ± 272	1,2,3
6:26:47.9	-54:24:06	13626 ± 30	1,2,3	6:28:30.0	-54:16:23	15412 ± 62	1,4
6:26:49.5	-54:32:34	15622 ± 58	1,2,3	6:28:34.6	-54:28:05	15564 ± 142	1,2
6:26:51.0	-54:32:48	15003 ± 40	1,2	6:28:46.8	-54:23:25	14313 ± 63	1
6:26:52.0	-54:28:52	15503 ± 64	1,2	6:28:49.1	-54:28:16	13447 ± 40	1
6:26:53.6	-54:35:07	15445 ± 95	1	6:28:57.2	-54:17:17	15847 ± 30	1,2
6:26:54.9	-54:19:14	14076 ± 101	1	6:29:00.2	-54:12:41	14836 ± 163	1,2
6:26:57.8	-54:33:31	15877 ± 31	1,2	6:28:59.7	-54:22:12	15088 ± 158	1,2
6:26:58.7	-54:28:09	15432 ± 92	1	6:28:59.8	-54:23:03	14561 ± 31	2
6:27:04.7	-54:25:47	15095 ± 146	1	6:29:03.0	-54:23:12	14977 ± 94	1,2,5,7
6:27:06.5	-54:22:15	15026 ± 180	1,2	6:29:09.9	-54:26:00	15003 ± 186	1,2
6:27:06.1	-54:33:26	15036 ± 159	1,2	6:29:27.0	-54:27:03	14678 ± 39	2
6:27:07.0	-54:26:40	16212 ± 113	1	6:29:33.4	-54:15:26	13311 ± 94	1,4
6:27:08.8	-54:05:31	15300 ± 34	1,2,3,4	6:29:37.2	-54:42:46	13856 ± 71	4
6:27:08.8	-54:22:25	16412 ± 39	1,2,3	6:29:44.7	-54:36:25	14510 ± 48	1,2
6:27:09.0	-54:26:45	14930 ± 77	1	6:29:47.1	-54:48:18	14912 ± 69	1,2,3
6:27:10.4	-54:20:08	15537 ± 113	1	6:29:47.6	-54:47:48	15110 ± 73	2,3
6:27:15.0	-54:00:03	15362 ± 88	1	6:30:06.6	-54:35:13	14506 ± 50	1
6:27:14.6	-54:08:34	16238 ± 69	1,4	6:30:09.9	-54:17:22	15243 ± 49	1
6:27:14.8	-54:25:34	14849 ± 72	1,2	6:30:15.6	-54:20:56	16162 ± 150	1
6:27:16.1	-54:23:00	16624 ± 32	1,2	6:30:24.3	-54:41:02	14686 ± 81	1
6:27:16.4	-54:32:07	15808 ± 31	1,2	6:30:25.4	-54:26:47	13911 ± 181	1
6:27:19.4	-54:06:58	17444 ± 36	1,4	6:30:25.6	-54:45:45	14970 ± 43	1,2
6:27:18.9	-54:24:06	15609 ± 123	4	6:30:29.3	-54:33:22	15377 ± 123	1
6:27:19.2	-54:25:15	13657 ± 40	1,4	6:30:28.9	-54:41:06	14959 ± 67	1
6:27:19.7	-54:28:31	14766 ± 262	1,4	6:30:36.3	-54:44:07	14312 ± 106	1
6:27:19.6	-54:37:00	14560 ± 80	4	6:30:51.2	-54:26:00	13432 ± 85	1
6:27:21.0	-54:26:20	16430 ± 30	1,2,4				

REFERENCES.— (1) Teague et al. 1990 with 82 km s^{-1} offset; (2) LCO-SHECTOGRAPH; (3) Hopp and Materne 1985; (4) CTIO-ARGUS with 50 km s^{-1} offset; (5) Materne et al. 1982; (6) West and Frandsen 1981; (7) Vidal 1975

TABLE 6
MASS DETERMINATIONS

Cluster	L^a (10^{45} ergs s^{-1})	$M_{gas}(\times 10^{14}$ M$_\odot$) 0.5 *Mpc*	1.0 *Mpc*	$n_e(0)$ (10^{-3} cm^{-3})	$M_{total}(\times 10^{14}$ M$_\odot$) 0.5 *Mpc*	1.0 *Mpc*	$\langle \frac{1}{r} \rangle^{-1}$ (Mpc)	M (10^1
A3528 SE	2.85	0.37	1.06	4.12	1.7	3.6	0.35(0.39)	7.29
A3528 NW	2.02	0.31	0.86	3.82	1.9	4.0	0.22	4
A1750 NE	1.72	0.28	0.90	1.72	1.3	2.7	0.20	1
A1750 SW	2.37	0.36	1.03	2.11	1.5	3.4	0.22	3
A3395 NE	2.07	0.30	1.00	1.38	1.6	3.8	0.23	4
A3395 SW	2.22	0.30	1.04	1.44	1.5	3.4	0.28	3

[a]Luminosities are from *ROSAT* data within 1 Mpc of each sub-cluster core.

[b]Virial Mass is determined from galaxies within a projected radius of 0.5 Mpc from the center of each sub-cluster.

TABLE 7
COMPOSITE VELOCITY RESULTS

Cluster	$\overline{v}$ (km s^{-1})	σ (km s^{-1})	V_r (km s^{-1})
Abell 3528	16346 ± 118	985 ± 101	
SE	16040 ± 318	$930 \pm 255(516 \pm 151)$[a]	96^{+379}_{-96}
NW	16136 ± 207	969 ± 198	
Abell 1750	25632 ± 132	1050 ± 96	
NE	24815 ± 153	676 ± 310	1335 ± 211
SW	26150 ± 145	906 ± 236	
Abell 3395	15177 ± 118	1069 ± 81	
NE all	15325 ± 167	949 ± 103	102^{+214}_{-102}
SW all	15427 ± 135	713 ± 185	
NE clip	15244 ± 165	1036 ± 107	192^{+236}_{-192}
SW clip	15436 ± 169	939 ± 311	

[a]The second velocity dispersion is after omitting the two highly discrepant members as discussed in the text.

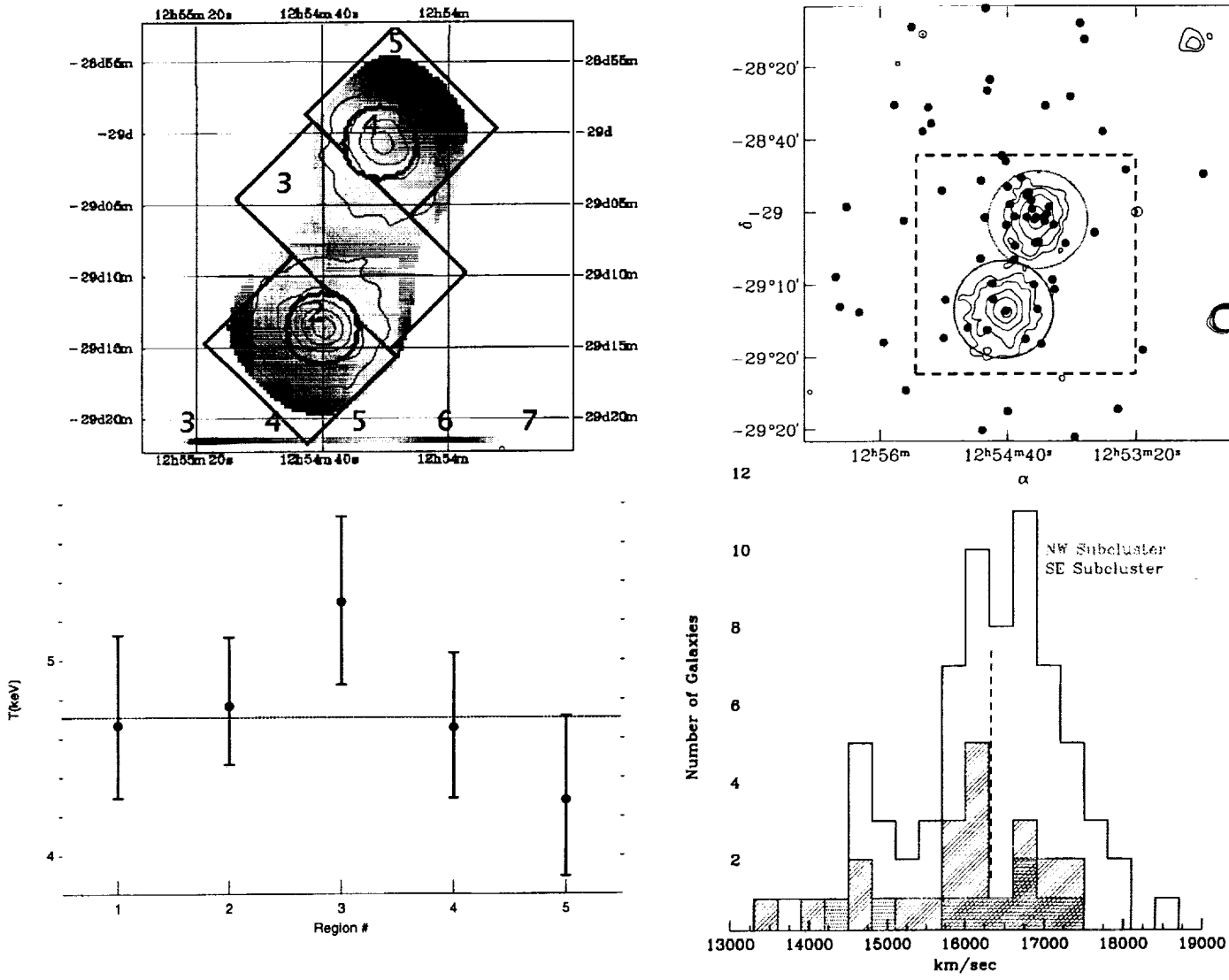

FIG. 1.— *Top left:* Continuous temperature map for A3528 from *ASCA* GIS data with intensity contours and region identifiers overlaid. *Bottom left:* Fit temperatures with 90% confidence error bars for the regions defined on the continuous temperature map. The global cluster temperature is show as a dotted line. *Top right:* Galaxies with redshifts are overlain on the *ROSAT* intensity contours. Galaxies with velocities greater than the overall mean cluster velocity are shown in red and those with smaller velocities are in blue. *Bottom right:* Velocity histogram of the galaxies shown in the top right. Bins are 300 km s^{-1} wide and the overall cluster velocity is indicated by a dashed line.

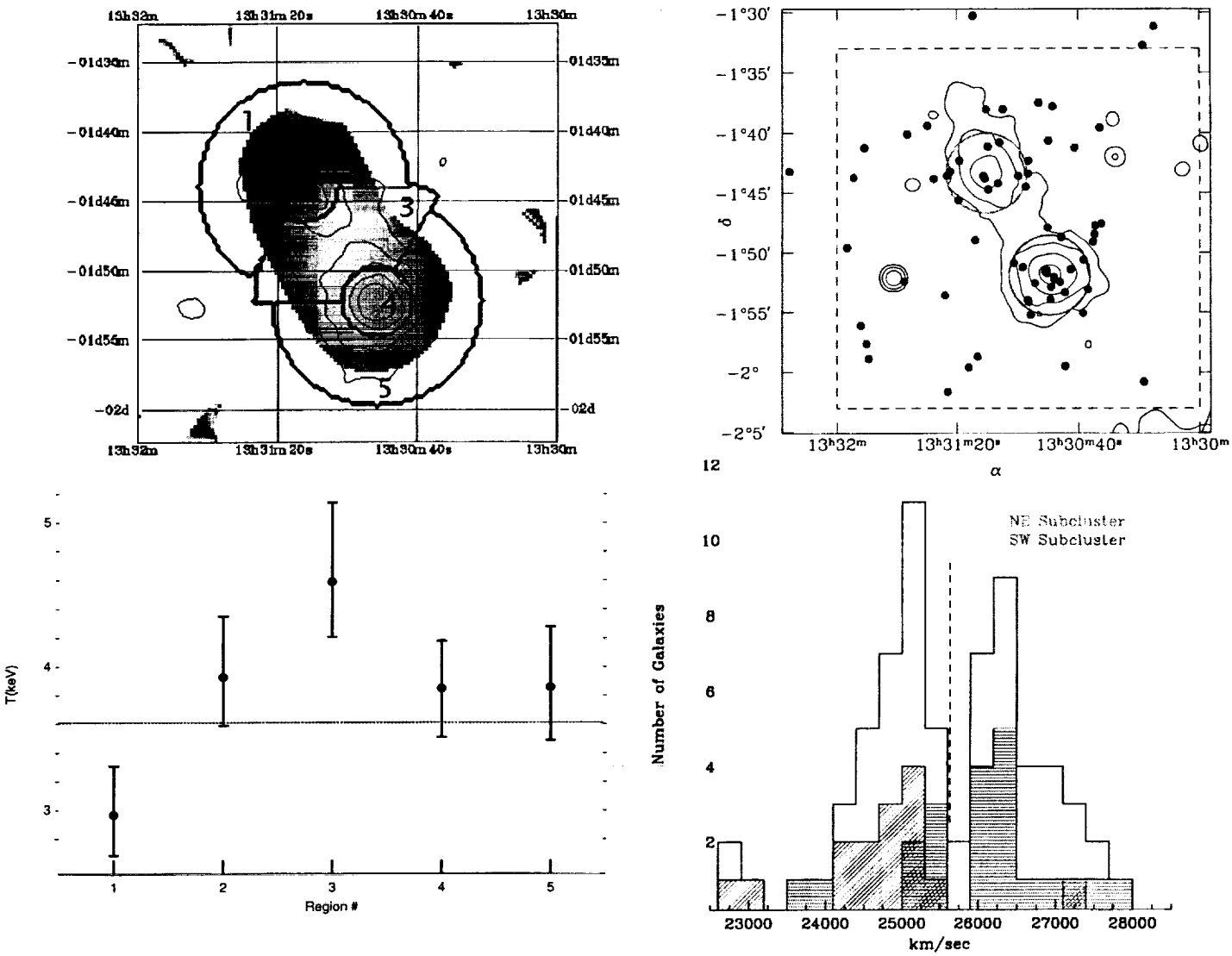

FIG. 2.— Same as for Figure 1 for Abell 1750. The field-of-view for the top right has been expanded to include all of the galaxies listed in Table 4 and shown in the lower right; the outline of the top left frame is shown as a dashed line.

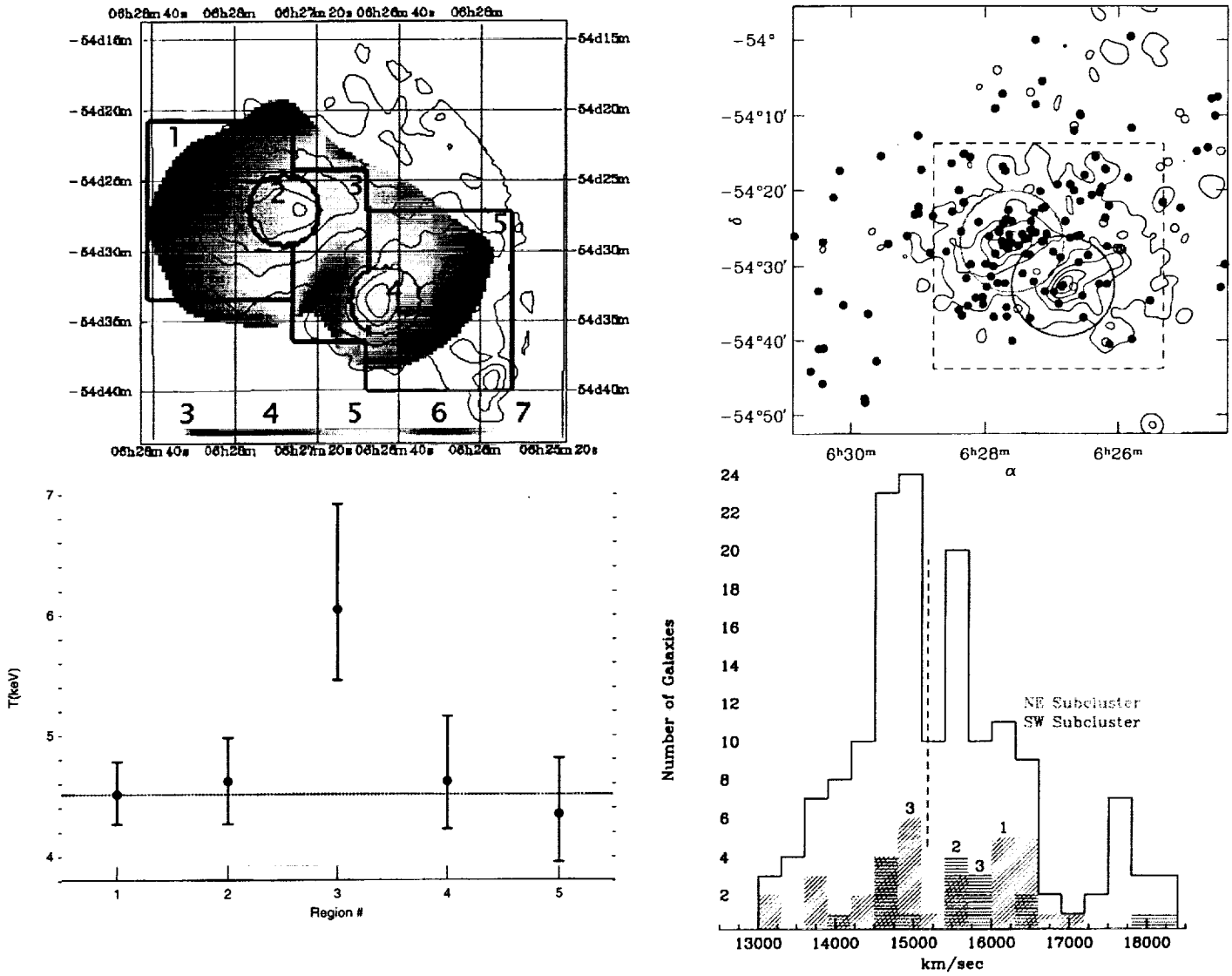

FIG. 3.— Same as for Figure 1 for Abell 3395. The field-of-view for the top right has been expanded to include all of the galaxies listed in Table 5 and shown in the lower right; the outline of the top left frame is shown as a dashed line. The galaxies in the high velocity bump in the bottom right are shown as empty circles in the top right panel.

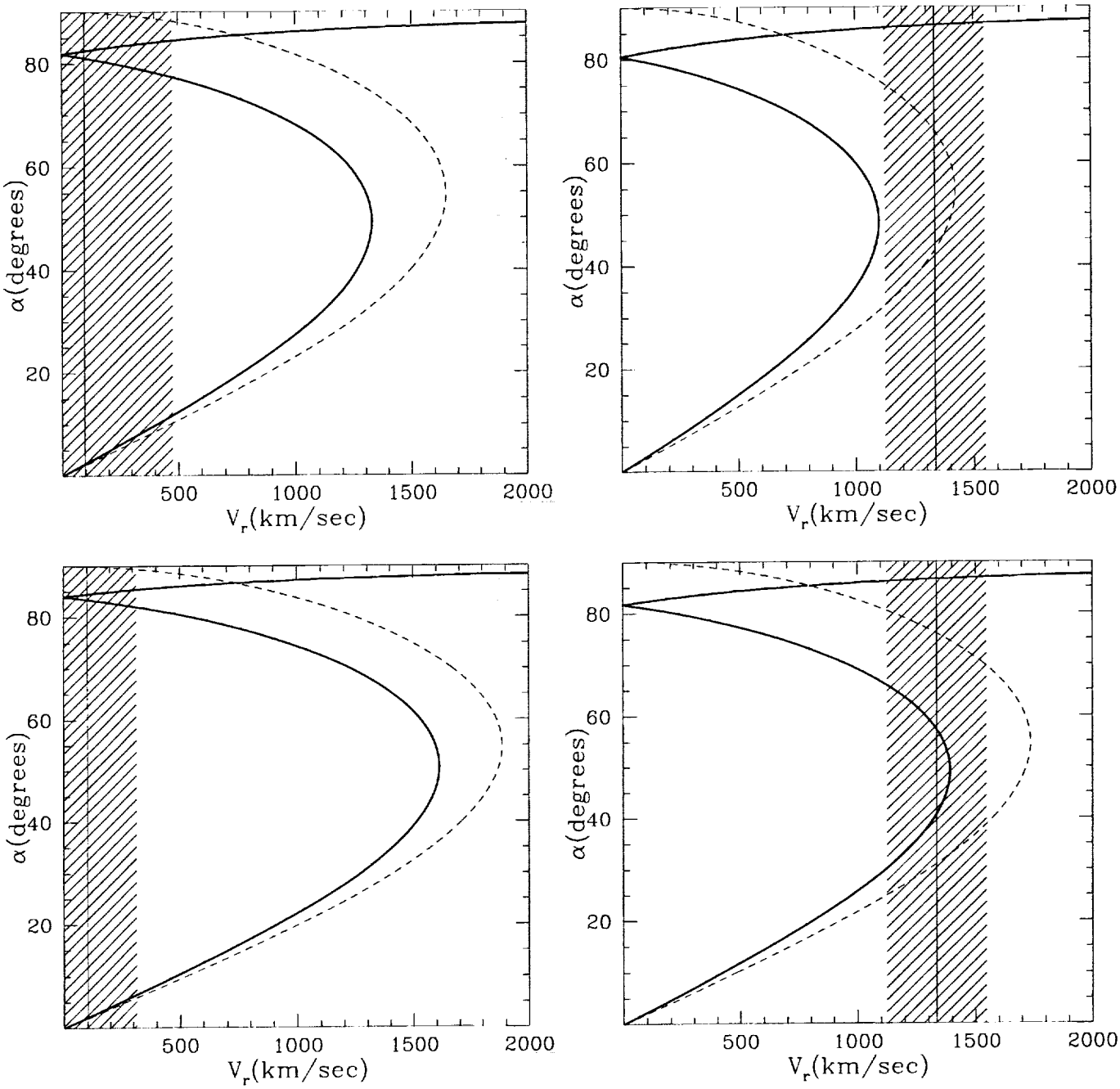

FIG. 4.— Solutions of the simplified equations of motion for Abell 3528 (*top left*), 1750 (*top right*) and 3395 (*bottom left*). Linear orbit solutions as a function of measured relative velocity (V_r) and inclination to the line of sight (α) are shown as the solid curve. The dashed line is the Newtonian binding condition, thus all orbit solutions to the right of the dashed line are unbound, while those to the left are bound. The measured relative velocity from our data is indicated by the solid vertical lines and its 68% confidence region is shown with the cross-hatching. For Abell 1750, we have also generated solution where the total mass has been increased by 50% (*bottom right*).